Numerical study of the effects of natural convection in a thermoacoustic device

O. Hireche[a], C. Weisman[a,b], D. Baltean-Carlès[a,b], V. Daru[a,c], Y. Fraigneau[a]

a. LIMSI-CNRS, Université Paris-Saclay, Rue John Von Neumann, 91405 Orsay, France
b. Sorbonne-Université, Faculté des Sciences et Ingénierie, 4 Place Jussieu, 75005 Paris, France
c. Laboratoire DynFluid, ENSAM, 151 Bd de l'Hôpital, 75013 Paris, France

Résumé :

On étudie les écoulements de convection naturelle dans un guide cylindrique contenant un milieu poreux. On retrouve cette configuration dans les moteurs thermoacoustiques à ondes stationnaires, composés d'un résonateur acoustique dans lequel un milieu poreux ou un stack (court) est positionné, en contact avec un échangeur de chaleur. Le gradient de température longitudinal, lorsqu'il est suffisamment fort, engendre le démarrage d'une onde acoustique. En thermoacoustique on néglige en général les effets de la convection naturelle et on suppose que les écoulements sont axisymétriques. Ici on réalise une étude numérique 3D des écoulements de convection naturelle à partir d'une résolution par volumes finis des équations de Navier-Stokes sous l'approximation de Boussinesq. On analyse l'effet de la variation des propriétés thermophysiques du milieu poreux (perméabilité, conductivité thermique, anisotropie) sur la structure de l'écoulement et le champ de température. L'écoulement est bien tri-dimensionnel et peut modifier de manière significative les conditions de démarrage et de fonctionnement du moteur thermoacoustique.

Abstract :

This study focuses on natural convection flows within a cylindrical guide containing a porous medium. This configuration is applicable to standing-wave thermoacoustic engines, usually composed of an acoustic resonator where a (short) stack (or porous medium) is inserted, with a heat exchanger placed at one of its ends. The resulting horizontal temperature gradient, when high enough, triggers the onset of an acoustic wave. Natural convection effects are usually neglected in thermoacoustics so that axisymmetry is often assumed. Here a 3D numerical study of natural convection flow is performed using a finite volume code for solving Navier-Stokes equations under Boussinesq approximation. The influence of the porous medium's physical characteristics (permeability, thermal conductivity, anisotropy) on the flow and temperature fields is investigated. It is shown that such flows are fully three-dimensional and therefore can modify significantly starting as well as steady operating conditions of the thermoacoustic engine.

Mots clefs : convection naturelle, milieu poreux, simulation numérique, thermoacoustique

Nomenclature

Latin		**Greek**	
c_p	heat capacity	α	thermal diffusivity
E_c	kinetic energy	β	expansion coefficient
e_h	heat exchanger thickness	ϵ	porosity
$\mathbf{e}_x$	unit vector in the vertical direction x	γ	thermal stratification ratio
H	reference height	λ	wavelength
K	permeability	μ	dynamic viscosity
k	thermal conductivity	ρ	density
L	length	**Subscript**	
p	nonhydrostatic pressure	c	cold
R, r	radius, radial coordinate	h	hot
Ra	Rayleigh number	max	maximum
T	temperature	p	porous medium
t	time	ref	reference
U, W	vertical, horizontal velocity	s	solid
$\mathbf{V}$	velocity vector		
X	phase variable		
x, y, z	spatial coordinates		

1 Introduction

In thermoacoustic devices, dynamic and thermal interactions between acoustic oscillations of a working gas and solid walls generate either heat pumping for refrigerating purposes or mechanical work for engine operating purposes. These devices represent an ecological alternative for industrial applications but they suffer from poor performance. This is generally caused by the existence of several nonlinear phenomena interfering with the process of energy transfer and penalizing the global performance of the device.

The energy conversion takes place in the vicinity of solid-fluid interfaces, and in order to increase the exchange surface, a porous medium is used for this conversion. The porous medium is a significant component of thermoacoustic devices and its characteristics greatly influence the device performance. The pores are usually of various shapes and sizes. In order to maintain the temperature distribution along the stack stable, thermal conductivity of the solid matrix should be lower than that of the working gas. Arnott et al. [1] developed a general thermoacoustic linear theory for the elements of thermoacoustic devices that have a microstructure and compared their performances. The porous media considered were solid stacks of plates or solids with many capillary tubes of circular, square or triangular geometry. They concluded that heat and work flows are approximately 10 percent greater for the parallel plate stack geometry than for other pore geometries. This model is still used in DeltaEC software [2], which is the reference code for computing a complete thermoacoustic system.

In thermoacoustic systems several nonlinear phenomena can take place, reducing their performance, such as : jet streaming, acoustic streaming, end effects and natural convection. These are not described yet or just partially. Among them, acoustic streaming has already been the subject of many studies during the last decades ([3], [4], [5]). Natural convection is a phenomenon that has mostly been neglected until

now in thermoacoustic applications, although it does exist because of the presence along the resonator of heat exchangers at different temperatures : two heat exchangers are generally placed at each end of the porous medium, in order to maintain a temperature gradient along the porous medium in thermoacoustic engines, or to benefit from heat pumping effects. Therefore, if the device is horizontal, there will be horizontal temperature gradients along the porous medium saturated with gas, as well as along the two cavities filled with gas on both sides of the porous medium. Natural convection flows can then develop as in differentially heated enclosures.

Natural convection in fluids and porous cavities has been treated extensively in the literature (see for example Nield and Bejan [6]). Heat transfer associated to natural convection flow in a partly porous cavity was studied by J.F Mercier et al. [7] in a 2D vertical cavity. A more recent study was conducted by Weisman et al. [8] in a geometry of a thermoacoustic engine. The goal was to predict the temperature distribution in a 2D differentially heated horizontal cavity, filled with a stack of plates which constitutes an anisotropic porous medium. This study showed that a darcean porous model gives correct orders of velocity scales, and allows for a qualitative description of the solutions. Some recent experimental studies of natural convection in thermoacoustic configurations investigate the influence of natural convection on Rayleigh streaming ([9], [10]).

In the present work, natural convection flows are investigated in a simplified geometry of a standing-wave thermoacoustic engine. A 3D numerical study of natural convection flow is performed using a finite volume code for solving Navier-Stokes equations under Boussinesq approximation. In the porous medium, the equations are modified using a Darcy term which becomes dominant as permeability decreases. The influence of the porous medium's physical characteristics (permeability, thermal conductivity, anisotropy) on the flow and temperature fields is investigated.

2 Model description

2.1 Geometry and boundary conditions

A simplified geometry for a standing-wave thermoacoustic engine is introduced : A horizontal cylindrical tube of length L and inner radius R, closed at both ends, is filled with air. A cylindrical porous medium of length L_p and radius R is inserted in the tube. In a standing-wave thermoacoustic engine, the fundamental mode is of wavelength $\lambda = 2L$. The porous medium length L_p is usually small compared to the wavelength, or equivalently $L_p \ll L$.

Attached to the "left" end of the porous medium (Fig. 1) is a hot heat exchanger (positioned at a distance L_L from the left end), which can be a coiled resistance modeled here as solid rings of width e_h maintained at given (hot) temperature T_h. Usually the "hot" part of the tube is insulated, and therefore in the present model, the longitudinal cylinder walls as well as the left end section are considered adiabatic. There is no cold heat exchanger in the present model, although there usually is one. Here the "cold" temperature is the ambient air temperature outside the cylinder, noted T_c. In the present model this cold temperature is imposed on the longitudinal cylinder walls as well as on the end section. Finally, a linear temperature profile is imposed on the tube wall around the porous medium. Thermal boundary conditions are shown on Figure 1 (bottom). At all solid-fluid interfaces, we assume continuity of temperature and heat flux as well as no slip conditions.

The porous medium is usually positioned inside the tube at about 1/8 of the total length. However, in this natural convection study, with the imposed boundary conditions, we have shown that the gas in the

right half of the tube is almost stagnant at cold temperature. Therefore it is not necessary to extend the computational domain too much. In the following simulations the porous medium will be positioned at about 1/4 of the total tube length.

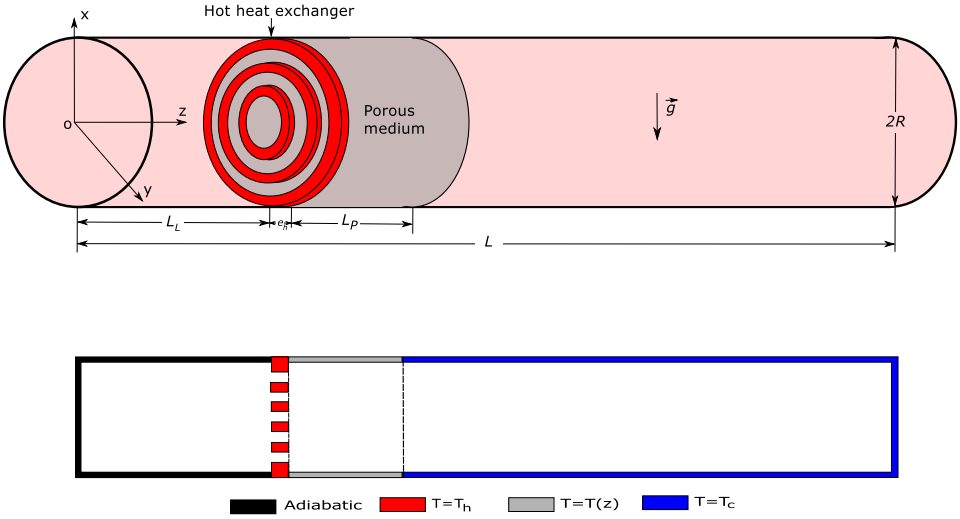

FIGURE 1 – Geometry (top) and thermal boundary conditions (bottom)

The porous medium, consisting of its solid matrix and the fluid pores is modeled as an equivalent homogeneous porous medium, with porosity ϵ, permeability tensor K, thermal conductivity tensor k_p. Also, it is common in thermoacoustics to use porous media composed of a solid (ceramic) matrix with horizontal cylindrical pores. In that case the porous medium is strongly anisotropic, and this possibility will also be considered.

2.2 Governing equations

In the fluid domain the Navier-Stokes equations are written as classically under Boussinesq assumptions. The reference gas density ρ, thermal conductivity k, heat capacity c_p, dynamic viscosity μ, and volume expansion coefficient at constant pressure $\beta = 1/T$ for an ideal gas are constant and equal to their value for cold temperature T_c.

In the porous medium, the momentum equations are modified using a Darcy term. A phase variable X is introduced to identify the nature of the medium ($X = 1$ for gas, $X = 0$ for the porous medium). Therefore the equations can be written in a unified form as :

$$\nabla.\mathbf{V} = 0 \tag{1}$$

$$\frac{\partial(\rho\mathbf{V})}{\partial t} + \nabla.(\rho\mathbf{V}\otimes\mathbf{V}) = -\nabla p + \mu\Delta\mathbf{V} + \rho g\beta(T-T_c)e_x - (1-X)\mu K^{-1}\mathbf{V} \tag{2}$$

$$\rho c_p\left(\frac{\partial T}{\partial t} + (\mathbf{V}.\nabla)T\right) = \nabla.(X\,k + (1-X)\,k_p)\nabla T \tag{3}$$

In the above equations $\mathbf{V}$ is the velocity vector, p is the nonhydrostatic pressure, T is the temperature, t is time, $\mathbf{e}_x$ is the unit vector in the vertical direction x and $\mathbf{g}$ is the acceleration of gravity.

2.3 Numerical solution

Computations are performed with the code SUNFLUIDH, which has been developped at LIMSI for simulations of unsteady incompressible or low Mach number flows.

The previous governing equations are solved using a finite volume approach with a 2nd order discretization in space and time. An implicit treatment of the viscous and thermal conductive terms ensures better numerical stability in regard to the time step which only depends on the CFL criterion. The equation set is solved by means of an ADI method [11]. An incremental projection method is used in order to ensure the divergence-free velocity field ([12],[13]). This implies to solve a Poisson's equation at each time step which is carried out with a multigrid-SOR algorithm [14]. The solution corresponds to the time-variation of pressure from which the correction term is estimated in order to get the divergence-free velocity field.

The mesh is body-fitted irregular, with 64 points regularly spaced along the radial direction, 48 points regularly spaced along the azimutal direction, and 256 points placed along the axis, with refined spacing near the heat exchanger and in the porous medium. The minimum and maximum mesh sizes in the axial direction are $\Delta z_{min} = 3.9{\cdot}10^{-4}m$ and $\Delta z_{max} = 4.2{\cdot}10^{-3}m$. In the radial direction, $\Delta r = 3.9{\cdot}10^{-4}m$. This spatial resolution is adequate for the given problem configurations.

The time step is adjusted throughout the simulation in order to satisfy a CFL<0.3 criterion.

3 Results

3.1 Reference configuration

The geometrical and thermal characteristics chosen for all cases are shown in Table 1. The thermophysical characteristics for air (fixed) and for the porous medium (for the reference case) are shown in Table 2. These parameters correspond (mostly) to some existing experiments in thermoacoustics [10]. The porous medium is considered to be isotropic, and the permeability and thermal conductivity tensors are reduced to scalar values. The equivalent thermal conductivity k_p is calculated from that of the solid matrix constituting the porous medium (k_s), the gas thermal conductivity and the porosity : $k_p = \epsilon k + (1-\epsilon)k_s$.

R	L	L_L	e_h	L_p	T_h	T_c
m	m	m	m	m	K	K
0.025	0.55	0.1	0.006	0.05	500	293

TABLE 1 – Geometrical and thermal parameters

ρ	μ	k	c_p	ϵ	K	k_p
$kg.m^{-3}$	$kg.m^{-1}s^{-1}$	$W.m^{-1}.K^{-1}$	$J.kg^{-1}.K^{-1}$		m^2	$W.m^{-1}.K^{-1}$
1.07	$1.9 \cdot 10^{-5}$	$2.8 \cdot 10^{-2}$	1004	0.84	10^{-6}	1.4

TABLE 2 – Reference configuration : thermophysical parameters for air and porous medium

The nondimensional parameter controlling natural convection is the Rayleigh number, which is classically calculated as $Ra = \frac{\rho g \beta \Delta T H^3}{\mu \alpha}$, with H a reference height, ΔT the imposed temperature difference, and $\alpha = \frac{k}{\rho c_p}$ the fluid thermal diffusivity [6]. The associated vertical velocity scale is $U_{ref} = \frac{\alpha}{H} Ra^{1/2}$. For the reference configuration, with $H = R$ and $\Delta T = 207K$, we find that $Ra = 2 \cdot 10^5$ and $U_{ref} = 0.48\, m/s$. The solution should be stationary. However the present configuration is not that

of fluid next to a simple vertical homogeneously heated plate, and it is unclear what values should be retained for the reference height and temperature difference.

In a fluid-porous cavity, we expect the presence of the porous medium to stabilize the flow and therefore a modified Rayleigh number is introduced, $Ra_p = \frac{\rho g \beta \Delta T H K}{\mu \alpha_p}$, with $\alpha_p = \frac{k_p}{\rho c_p}$ the porous medium equivalent thermal diffusivity [6]. The associated vertical velocity scale is $U_{refp} = \frac{\alpha_p}{H} Ra_p$. For the reference configuration, $Ra_p = 6.71$, $U_{refp} = 0.35\, m/s$ and we expect a stationary solution of the natural convection problem. Again it is unclear what values should be retained for H and ΔT.

3.2 Numerical results for the reference configuration

The flow and temperature fields are first described in the reference configuration presented in the previous section. They are fully three-dimensional. Figure 2 shows on the vertical middle plane section the velocity vectors with contours of axial velocity (Fig. 2a) and contours of temperature (Fig. 2b). White dotted lines show the extent of the porous medium. The flow and temperature fields on this plane are characteristic of natural convection in a differentially heated fluid cavity on the left of the heat exchanger (with adiabatic conditions on all boundaries except for the heat exchanger section). On the right of the heat exchanger, the flow and temperature field resemble that of natural convection in a differentially heated porous-fluid cavity (with prescribed temperature on all boundaries). However the heat exchanger is not a wall, and therefore there is fluid passing from one cavity to the other. Also the heat exchanger is not ideal, and the condition $T = T_h$ is not imposed homogeneously on the cross-section.

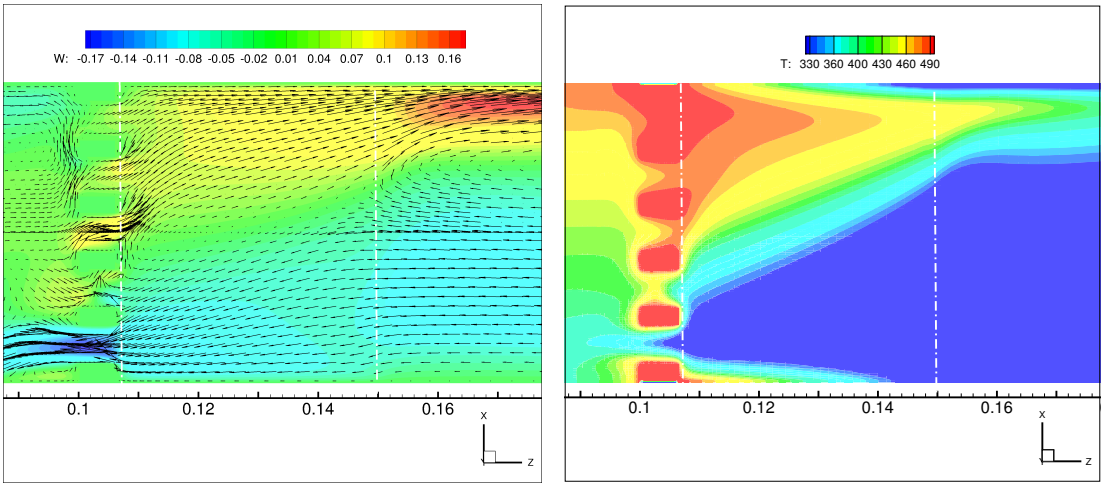

(a) (b)

FIGURE 2 – Reference configuration, vertical middle plane section : (a) Velocity vectors with contours of axial velocity, (b) Contours of temperature (white dotted lines show the extent of the porous medium).

Figure 3 shows on several vertical cross-sections the contours of vertical velocity (left) and of temperature (right). The corresponding cross sections are shown on the sketch at the bottom of Figure 3. The flow and temperature fields at $z = z_1$ (Fig. 3.ab1), on the left of the heat exchanger, are characteristic of natural convection flow in a differentially heated cylindrical cavity, with adiabatic boundaries. On a section cutting through the heat exchanger, at $z = z_2$ (Fig. 3.ab2) the flow is constrained between the solid rings that constitute the heat-exchanger, and hot temperature T_h is maintained on the rings. On a section cutting through the porous medium, at $z = z_3$ (Fig. 3.ab3), the flow and temperature field are essentially characteristic of natural convection in a differentially heated porous cylindrical cavity, with fixed temperature on the tube wall. Finally, on the right part of the porous medium, at $z = z_4$ (Fig. 3.ab4),

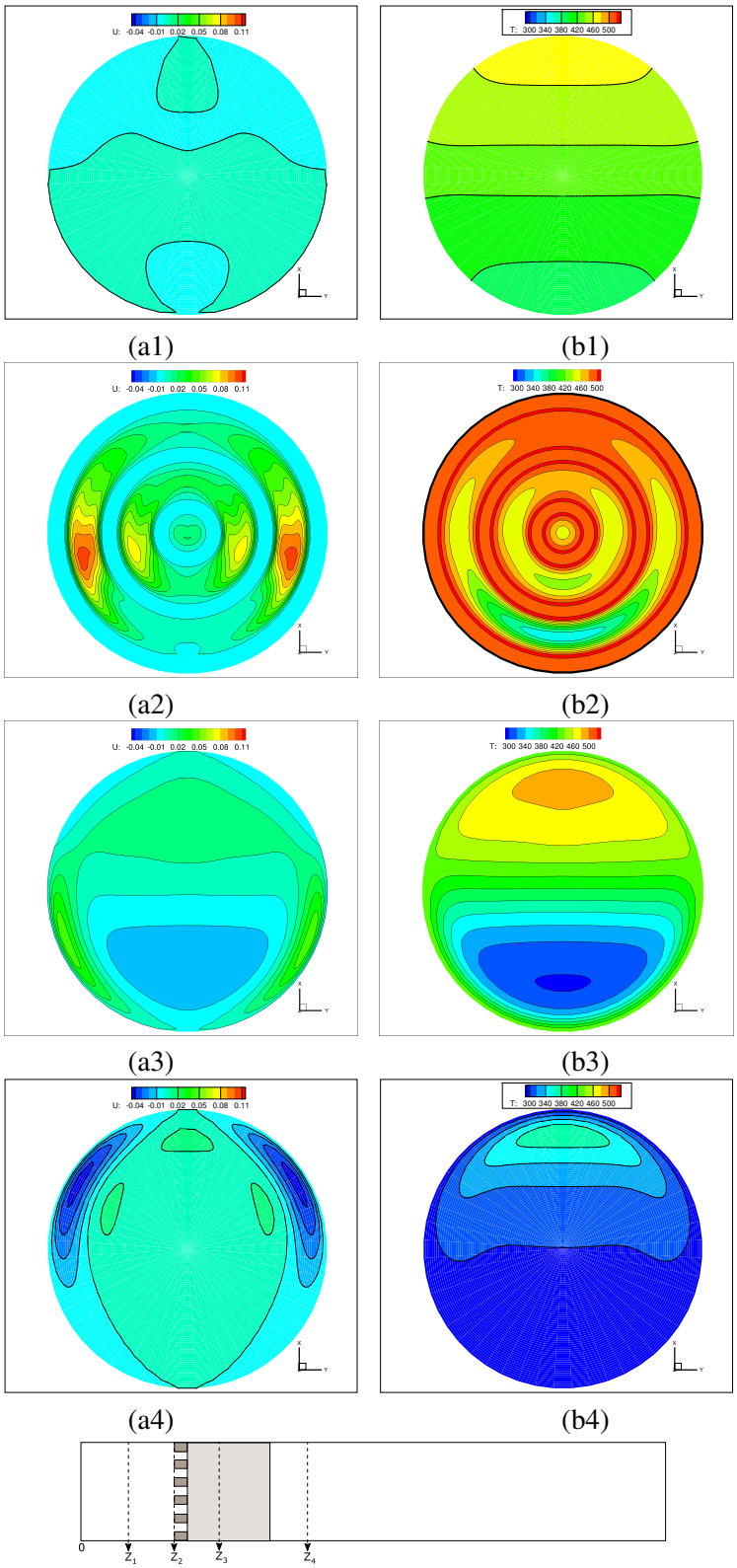

FIGURE 3 – Reference configuration, contours of (a) vertical velocity and (b) temperature, for (1) $z_1 = 0.05m$, (2) $z_2 = 0.101m$, (3) $z_3 = 0.12m$, and (4) $z_4 = 0.2m$. Locations of z_1 to z_4 are shown on the sketch at the bottom of the figure.

natural convection flow within a fluid cavity with cold temperature on the boundaries is recovered. The flow is slower and the temperature field becomes more homogeneously cold. There is a clear symmetry

of flow and temperature with respect to the vertical axis in all figures. The maximum vertical velocity $U_{max} = 0.115m/s$ is read on the scale of Fig. 3. The maximum axial velocity $W_{max} = 0.17m/s$ is read on the scale of Fig. 2a. These are of the same order of magnitude than the reference velocity scales U_{refp} and U_{ref} calculated in the previous section.

3.3 Parametric study

In this section, several parameters characterizing the porous medium are varied, keeping a fixed porosity : permeability, anisotropy, equivalent thermal conductivity.

In order to analyse the influence of each parameter, we define several flow and temperature output parameters : The maximum vertical velocity amplitude in the tube is noted U_{max} and $(x_{max}, y_{max}, z_{max})_U$ is the corresponding location. The maximum axial velocity amplitude in the tube is noted W_{max} and $(x_{max}, y_{max}, z_{max})_W$ is the corresponding location. The total kinetic energy within the tube is noted E_c. Also, the ratio of vertical versus horizontal temperature gradient in the core of the porous medium is noted $\gamma = |\frac{\partial T}{\partial x}|/|\frac{\partial T}{\partial z}|$. It is a measure of the strength of natural convection : If conduction is dominant $\gamma \to 0$, and if convection is dominant $\gamma \to \infty$.

The value of the permeability K depends on the geometry of the porous medium. In the following paragraph, it is varied between $10^{-2}\ m^2$ (very permeable) and $10^{-8}\ m^2$ (very impermeable), considering the porous medium to be homogeneous and isotropic.

Table 3 presents the results for 4 different values of the porous medium permeability, when the porous medium is isotropic. As K decreases, the total kinetic energy and the γ ratio also decrease, which is to be expected because the porous medium acts more and more like a solid barrier and natural convection flow looses strength. It is interesting to note that the maximum vertical velocity decreases, and that its location shifts from just right of the heat exchanger (on the central horizontal plane, facing the middle of the outer heat exchanger fluid space) to just outside the porous medium as permeability decreases (slightly higher than the tube center). The maximum axial velocity also decreases with K, and its location (in the right fluid cavity, on the central vertical plane, facing the middle of the outer heat exchanger fluid space) shifts to just outside the porous medium as permeability decreases. This is consistent with natural convection flow developing outside of the porous medium when K is very small. The orders of magnitude of the maximum velocities vary with the value of K, but not proportionally as in a simpler configuration with natural convection through a porous medium (see the reference velocity scales U_{ref} and U_{refp} presented in the previous section).

K	U_{max}	$(x_{max}, y_{max}, z_{max})_U$	W_{max}	$(x_{max}, y_{max}, z_{max})_W$	E_c	γ
m^2	$m.s^{-1}$	(m, m, m)	$m.s^{-1}$	(m, m, m)	J	
10^{-2}	0.20	$(0, \pm 5R/6, 0.110)$	0.28	$(5R/6, 0, 0.170)$	$2.32 \cdot 10^{-3}$	15.5
10^{-4}	0.20	$(0., \pm 5R/6, 0.108)$	0.27	$(5R/6, 0, 0.172)$	$2.15 \cdot 10^{-3}$	11.1
10^{-6}(ref)	0.12	$(R/12, \pm 5R/6, 0.104)$	0.17	$(5R/6, 0, 0.178)$	$5.17 \cdot 10^{-4}$	1.9
10^{-8}	0.05	$(3R/7, 0, 0.152)$	0.05	$(5R/6, 0, 0.164)$	$2.16 \cdot 10^{-5}$	0.168

TABLE 3 – Effect of variation of permeability, isotropic porous medium

Figure 4 shows on the vertical middle plane section, for $K = 10^{-2}$ the velocity vectors with contours of axial velocity (Fig. 4a) and contours of temperature (Fig. 4b). White dotted lines show the extent of the porous medium. It is clear on this figure that the fluid flows freely through the porous medium.

On the right of the heat exchanger, the fields correspond to natural convection in a fluid cavity, with prescribed temperature on the boundaries. The maximum velocities U_{max} and W_{max} (Table 3) are of the same order of magnitude but smaller than U_{ref} calculated in Section 3.1. This is probably due to the cylindrical geometry, the choice of thermal boundary conditions and the imperfect heat exchange on the hot heat exchanger. On the left of the heat exchanger, fields correspond to natural convection in a fluid cavity, with adiabatic boundaries except for the heat exchanger section.

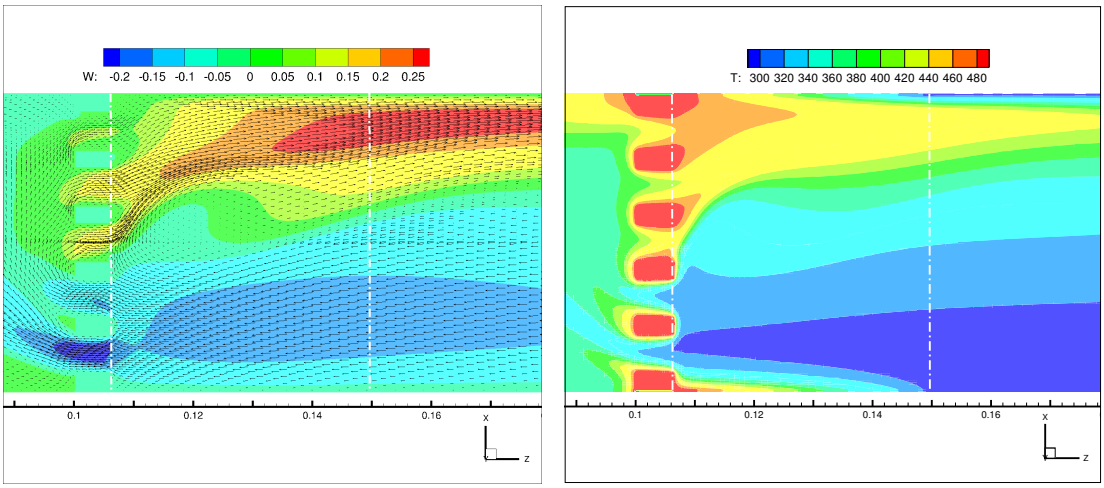

(a) (b)

FIGURE 4 – Isotropic porous medium, $K = 10^{-2}$, vertical middle plane section : (a) Velocity vectors with contours of axial velocity, (b) contours of temperature (white dotted lines show the extent of the porous medium).

Figure 5 shows on the vertical middle plane section, for $K = 10^{-8}$ the velocity vectors with contours of axial velocity (Fig. 5a) and contours of temperature (Fig. 5b). White dotted lines show the extent of the porous medium. It is clear on this figure that the porous medium behaves almost like a conducting solid. On the right end of the porous medium, the temperature is only slightly higher than T_c, so that convection is greatly diminished and the maximum velocities U_{max} and W_{max} are much smaller (on the order of $0.05m/s$, which corresponds to the fluid velocity scale U_{ref} for $H = R$ and $\Delta T = 2K$). On the left of the heat exchanger, the temperature is almost homogeneous (equal to T_{hot}) and there is almost no flow.

The equivalent porous medium thermal conductivity is varied next, for homogeneous isotropic porous media, keeping all other parameters corresponding to the reference case. Four values were tested, from $k_p = 0.028$ to $k_p = 1.4W.m^{-1}.K^{-1}$, based on studies of porous media used in thermoacoustics [15]. It was shown that the flow and temperature field variation is negligible.

Anisotropy is considered next : in the case of pores that are horizontal capillary tubes, the porous medium is almost impermeable in the transverse direction, so that $K_{xx} \simeq 0$. The permeability in the axial direction K_{zz} is varied between $10^{-2}\,m^2$ and $10^{-8}\,m^2$. For the present study the equivalent porous medium thermal conductivity is assumed to be identical in all directions. Figure 6 shows for the anisotropic case, $K_{zz} = 10^{-6}\,m^2$, all other parameters being maintained the same as in the reference configuration, on the vertical middle plane section the velocity vectors with contours of axial velocity (Fig. 6a) and contours of temperature (Fig. 6b). The flow structure is strongly modified inside the porous medium, since it is constrained horizontally and flows through the fluid space between the heat exchanger rings (compare with Fig. 2a). The temperature field is also modified (compare with Fig. 2b). The solution

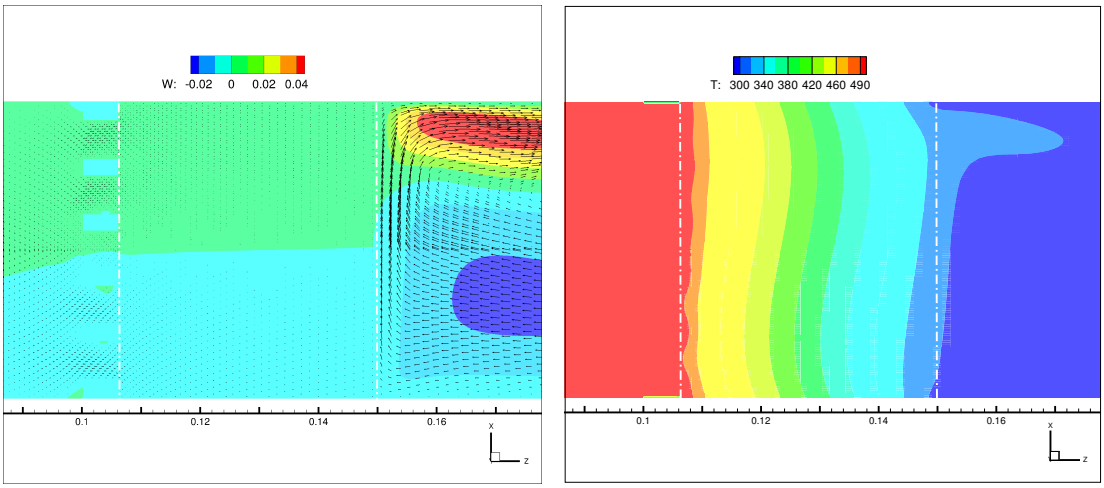

(a) (b)

FIGURE 5 – Isotropic porous medium, $K = 10^{-8}$, vertical middle plane section : (a) Velocity vectors with contours of axial velocity, (b) contours of temperature (white dotted lines show the extent of the porous medium).

inside the porous medium is analogous to natural convection flow in a shallow horizontal cavity, with on the top half hot fluid flowing to the right, and on the bottom half cold fluid flowing to the left. Then on the right of the porous medium, a more standard natural convection fluid cavity flow is recovered. For this configuration, the maximum vertical velocity is $0.12m/s$ measured at $(x = R/2, y = 0, z = 0.151m)$ (just on the right of the porous medium), and the maximum axial velocity is $0.17m/s$ measured at $(x = 9R/10, y = 0, z = 0.165m)$ (also on the right of the porous medium). The total kinetic energy is $E_c = 2.84 \cdot 10^{-4}\, J$ (smaller than in the reference configuration) but the ratio γ is equal to $\gamma = 4.56$ (larger than in the reference configuration).

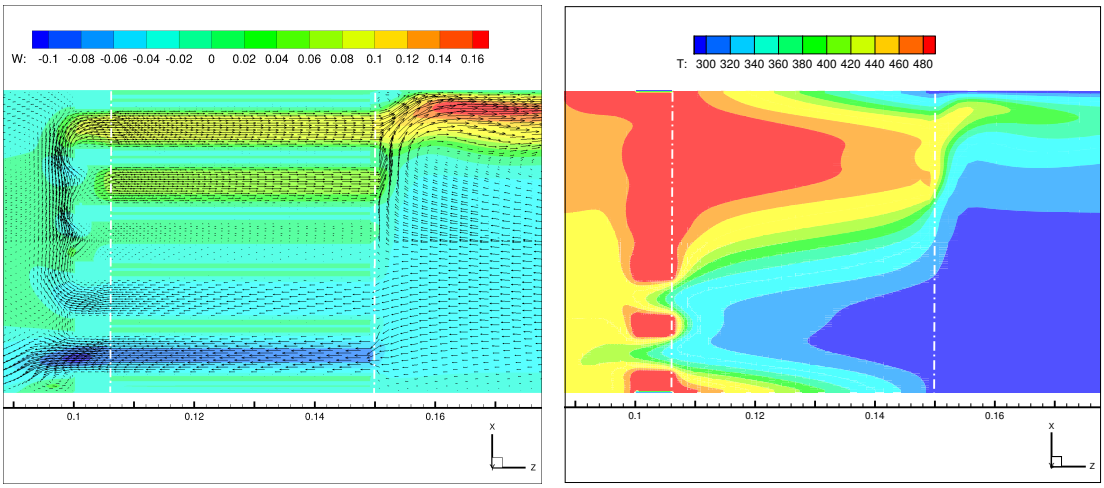

(a) (b)

FIGURE 6 – Anisotropic porous medium, $K_{zz} = 10^{-6}$, on the vertical middle plane section : (a) Velocity vectors with contours of axial velocity, (b) contours of temperature (white dotted lines show the extent of the porous medium).

3.4 Consequences for thermoacoustic applications

The previous simulations of natural convection flows were performed on configurations (geometry, materials, choice of fluid, applied temperature differences) applicable to thermoacoustic engines, even though there was no acoustics.

Based on these simulations and observations, steady natural convection flows should not be neglected in the design of standing-wave thermoacoustic engines. The onset of an acoustic wave is based on the existence of a temperature gradient regularly distributed along the porous medium. Since natural convection flows induce very distorted temperature fields, they can delay or even prevent the onset of acoustic waves. Natural convection flows could interfere with acoustics, and also with other nonlinear phenomena occuring in such thermoacoustic devices, such as streaming flow. It would be interesting to run some simulations of acoustics and natural convection together, but these have to be three-dimensional, with no axisymetry assumed.

Finally such flows may have applications for other devices involving thermoacoustics, such as thermoacoustic heat pumps or traveling-wave thermoacoustic engines, as long as there is a horizontal temperature difference between the constituting elements.

4 Conclusion

A three-dimensional numerical study of natural convection flow was performed using a finite volume code for solving Navier-Stokes equations under Boussinesq approximation, in a configuration applicable to thermoacoustic devices. The influence of the porous medium's physical characteristics (permeability, thermal conductivity, anisotropy) on the flow and temperature fields was investigated. It was shown that such flows are fully three-dimensional and can modify significantly starting as well as steady operating conditions of the thermoacoustic engine. Simulations of both acoustics and natural convection in thermoacoustic configurations are in progress, in order to analyse their interaction.

Acknowledgements

This work was partly financed by ANR project TACOT (Projet-ANR-17-CE06-0007).

Références

[1] W. P. Arnott, H. E. Bass, and R. Raspet, General formulation of thermoacoustics for stacks having arbitrarily shaped pore cross sections, J. Acoust. Soc. Am., 90 (1991) 3228–3237.

[2] W.C Ward, J. Clark, and G.W. Swift, Design Environment for Low-amplitude Thermoacoustic Energy Conversion (DeltaEC Version 6.2), Users Guide, 2008.

[3] M. W. Thompson, A. A. Atchley, and M. J. Maccarone, Influences of a temperature gradient and fluid inertia on acoustic streaming in a standing wave, J. Acoust. Soc. Am., 117 (2005), 1839–1849.

[4] I. Reyt, V. Daru, H. Bailliet, S. Moreau, J.C. Valière, D. Baltean-Carlès and C. Weisman, Fast acoustic streaming in standing waves : Generation of an additional outer streaming cell, J. Acoust. Soc. Am., 134 (3) (2013) 1791-1801.

[5] V. Daru, D. Baltean-Carlès, C. Weisman, P. Debesse and G. Gandikota, Two-dimensional numerical simulations of nonlinear acoustic streaming in standing waves, Wave Motion, 50 (2013) 955-963.

[6] D.A. Nield, A. Bejan, Convection in Porous Media, Springer and Business Media, New York, 2006.

[7] J.-F. Mercier, C. Weisman, M. Firdaouss and P. Le Quéré, Heat transfer associated to natural convection flow in a partly porous cavity, Journal of Heat Transfer, 124 (1) (2002) 130–143.

[8] C. Weisman, D. Baltean-Carlès, P. Duthil, P. Le Quéré, Natural convection in a stack of horizontal plates in a differentially heated cavity, in : S. Brynjolfsson, O. P. Palsson, J. H. Kim (ed.) Proceedings of the 19th International Symposium on Transport Phenomena (ISTP-19), Published by University of Iceland Faculty of Industrial Engineering, Mechanical Engineering and Computer Science Reykjavik, Island, 2008.

[9] E. Saint Ellier, Y. Bailly, L. Girardot, D. Ramel and P. Nika, Temperature gradient effects on acoustic and streaming velocities in standing acoustic waves resonator, Experimental Thermal and Fluid Science, 66 (2015) 1–6.

[10] I. Ramadan, H. Bailliet and J.-C. Valière, Experimental investigation of the influence of natural convection and end-effects on Rayleigh streaming in a thermoacoustic engine, J. Acoust. Soc. Am., 143(1) (2018) 361–372.

[11] D. W. Peaceman, H. H. Rachford, The numerical solution of parabolic and eliptic differential equations, J. Soc. Indust. Appl. Math., 3 (1955) 28–41.

[12] K. Goda, A multistep technique with implicit difference schemes for calculating two or three-dimensional cavity flows, J. Comput. Phys., 30 (1979) 76–95.

[13] J. L. Guermond, P. D. Minev, J. Shen, An overview of projection methods for incompressible flows. Comp. Meth. Appl. Mech. Eng., 195 (2006) 6011–6045.

[14] Y. Saad, Iterative Methods for Sparse Linear Systems, 2nd Edition, Society for Industrial and Applied Mathematics, 2003.

[15] S. H. Tasnim, Porous Media Thermoacoustic Stacks : Measurements and Models. Thesis, University of Waterloo, Ontario, Canada, 2011.